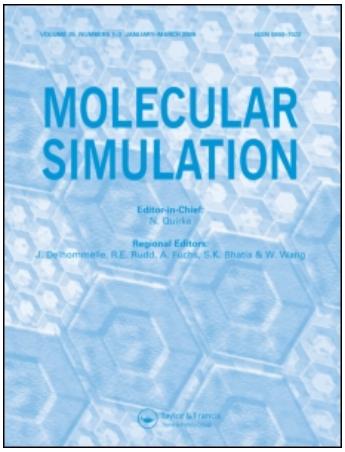

Molecular Simulation
Publication details, including instructions for authors and subscription information:
http://www.informaworld.com/smpp/title~content=t713644482

Mechanics of silicon nanowires: size-dependent elasticity from first principles

R. E. Rudd[a]; B. Lee[a]
[a] Lawrence Livermore National Laboratory, University of California, Livermore, CA, USA

To cite this Article Rudd, R. E. and Lee, B.(2008) 'Mechanics of silicon nanowires: size-dependent elasticity from first principles', Molecular Simulation, 34: 1, 1 — 8
To link to this Article: DOI: 10.1080/08927020701730435
URL: http://dx.doi.org/10.1080/08927020701730435

Molecular Simulation
Vol. 34, No. 1, January 2008, 1–8

Taylor & Francis
Taylor & Francis Group

Mechanics of silicon nanowires: size-dependent elasticity from first principles

R.E. Rudd* and B. Lee

Lawrence Livermore National Laboratory, University of California, L-045, Livermore, CA 94551, USA

(Received 24 August 2007; final version received 6 October 2007)

We discuss size-dependent elastic properties in the context of our recent work on the mechanics of silicon nanowires. The results are based on first-principles density functional theory calculations. We focus especially on the size dependence of the Young's modulus, but also comment on the size dependence of the residual stress and the equilibrium length of the hydrogen-passivated Si nanowires. We compare these results to prior results from classical molecular dynamics based on empirical potentials.

Keywords: nanowire; Young's modulus; density functional theory; size effect; surface stress

1. Continuum elasticity at the nanoscale?

Does continuum elastic theory (and more generally continuum mechanics) work for nanoscale systems? Are the mechanical properties of a nanoscale material the same as those listed in handbooks and compendia for the same material in macroscopic systems? If a material constant becomes size dependent in small systems, at what sizes does the deviation from the bulk value begin to be important? And conversely, over what size ranges is the unadulterated macroscopic theory valid? These are clearly important questions since we would like to be able to apply the well developed continuum mechanical theory with confidence to nanoscale systems. Deformation under load, yielding, fracture, fatigue and friction are but a few topics of continuum mechanics that may be determining factors in the function or failure of a nanoscale device. Here, we focus on the first topic, elastic deformation, since we are in a position to address it from first principles using quantum mechanical theory.

It has been long recognized in conventional materials science that material heterogeneity can cause size-dependent mechanical properties. For example, the surface properties of cast metals may differ significantly from those of the interior, such as the hardening of the surface in chilled cast iron that is used to improve its wear properties [1]. The material properties depend on the relative fraction of the surface and interior region, and are thus size dependent. This macroscopic effect is tied to differences in the microstructure at the surface of the cast part and the increasing proportion of the hardened material as the size of the sample is reduced. At first glance, it may seem that there is nothing heterogeneous about a defect-free single crystal nanowire; however, the *surface itself is a heterogeneity*. The atoms at the surface are not the same as those in the bulk. The coordination of the atoms at the surface is less than that of those in the bulk. In an effort to minimize the decrease in coordination, the atomic bonds may distort to form a reconstructed surface or different molecules may attach and fill the dangling bonds at the surface. Both the reduced coordination and the bond distortion change the character of all of the bonds of the surface atom, as may be quantified through the bond order, for example. These deviations from bulk bonding propagate some distance into the bulk. The presence of this surface layer whether intrinsic or extrinsic gives rise to the size dependence of the mechanical properties, both through changes in the equilibrium bond lengths showing up as surface stresses and changes in the surface elastic constants. It is natural to expect then that the thickness of this surface layer in which the mechanical properties are modified sets the length scale of the size dependence.

We are particularly interested in the size dependence of the Young's modulus because of its importance in rod-like structures. To understand how the size dependence arises in an archetypal system consider a cylinder of total radius R comprised of a homogeneous, isotropic material in the middle or core of the cylinder covered by a uniform layer of a different homogeneous, isotropic material of thickness t at the surface. The core and surface are taken to have different mechanical properties; for example, their Young's moduli are E_{core} and E_{surf}, respectively. The Young's modulus is the ratio of the stress applied along the longitudinal axis of the cylinder to the resulting strain of elongation ε.

The surface contributes to the Young's modulus of the whole, composite wire, E_{tot}, leading to a size dependence as discussed previously in the literature

*Corresponding author. Email: robert.rudd@llnl.gov

ISSN 0892-7022 print/ISSN 1029-0435 online

DOI: 10.1080/08927020701730435
http://www.informaworld.com

(cf. Refs. [2–4]). Both the core and the outer shell of material undergo the same longitudinal strain and the surface is traction-free. Suppose the Poisson ratios of the two materials are the same, or close enough that the compatibility condition may be neglected akin to a Taylor approximation. Then, the stress in each material is the product of its (bulk) Young's modulus and the longitudinal strain. Since the total force supported by the cylinder is the sum of the force carried by each region and that force is the product of the axial stress and the cross-sectional area over which it acts, we arrive at the Equation for the composite Young's modulus $E_{\rm tot}$:

$$A_{\rm tot}E_{\rm tot}\varepsilon = A_{\rm core}E_{\rm core}\varepsilon + A_{\rm surf}E_{\rm surf}\varepsilon, \tag{1}$$

where the areas are given by $A_{\rm tot} = \pi R^2$, $A_{\rm core} = \pi[(R-t)^2] = A_{\rm tot}(1 - C_{\rm tot}t/A_{\rm tot}) + \mathcal{O}(t^2/R^2)$ and $A_{\rm surf} = \pi[R^2 - (R-t)^2] = C_{\rm tot}t + \mathcal{O}(t^2/R^2)$, where $C_{\rm tot}$ is the circumference of the cylinder. If we assume that the outer layer is very thin, $t \ll R$, then we have

$$E_{\rm tot} = E_{\rm core}\left(1 + \frac{2t}{R}\Delta\right) + \mathcal{O}(t^2/R^2), \tag{2}$$

$$= E_{\rm core}\left(1 + \frac{C_{\rm tot}t}{A_{\rm tot}}\Delta\right) + \mathcal{O}(t^2/R^2), \tag{3}$$

where $\Delta = (E_{\rm surf} - E_{\rm core})/E_{\rm core}$ is a measure of the difference in the properties of the core and the surface[1]. For nanoscale systems, it is not a simple matter to determine the surface Young's modulus $E_{\rm surf}$ from experiment. It should be clear, however, that the Young's modulus of the composite system is size dependent, scaling like $1/R$. The size scale is set by the product $2t\Delta$, which is independent of the size of the cylinder. The cylinder's surface area to volume ratio is equal to $C_{\rm tot}/A_{\rm tot}$, scaling like $1/R$, and it is evident that to this leading order in t/R the leading size-dependent term scales like the surface area to volume ratio for any beam regardless of the shape of the cross section. We conclude that it is natural to expect the Young's modulus of a beam to become significantly size dependent as the diameter of the beam approaches the characteristic length scale set by the thickness of the surface layer.

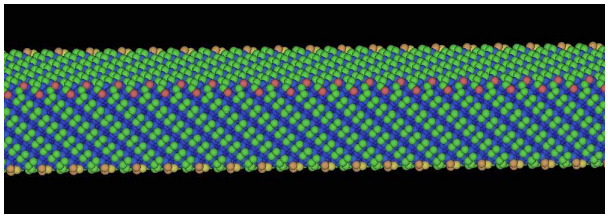

Figure 1. Image of the 3-nm silicon nanowire showing the 2×1 {100} dimer reconstruction for the SW potential. Calculation of the Young's modulus involves expanding the periodic box in the wire's longitudinal direction, allowing the wire to relax to mechanical equilibrium in the transverse directions, and calculating the resulting axial stress. Each sphere represents a Si atom, colored according to that atom's energy at zero temperature.

The Young's modulus controls the mechanical behavior of beams in other situations, too. For example, the modulus enters formulas for bending and fracture. Since bending is often used to measure the Young's modulus, it may be helpful to note that the size dependence in bending is similar to, but not exactly the same as, that in elongation since the different surfaces experience different strains, the convex surface in tension and the concave surface in compression, with the strain varying linearly across the side walls of a rectangular beam. In particular, the bending modulus $\kappa_{\rm b}$ is the ratio of the bending moment, M, to the resulting curvature, $\kappa = 1/\rho$ (where κ is the reciprocal of the radius of curvature, ρ)

$$M = \kappa_{\rm b}\kappa. \tag{4}$$

In classical beam theory $\kappa_{\rm b} = EI$, the product of the Young's modulus and the moment of inertia [5]. The size dependence of the bending modulus can be calculated in linear isotropic elasticity in much the same way it was calculated for the Young's modulus above, but for bending it is the relative contribution of the surface and core to the moment of inertia that is essential, rather than the relative area [4]. We focus on a rectangular beam with height h in the bending direction, width w and a uniform surface layer of thickness t. Using the Taylor-like approximation that neglects compatibility, the result for the bending modulus is

$$\kappa_{\rm b} = E_{\rm core}I\left[1 + \left(6\frac{t}{h} + 2\frac{t}{w}\right)\Delta\right], \tag{5}$$

$$I = \int {\rm d}x\,{\rm d}y\,y^2 = \frac{1}{12}wh^3, \tag{6}$$

where Δ is defined as above. Thus, the bending modulus also shows a size effect that is inversely proportional to the thickness of the beam. The size dependence of the bending modulus is quantitatively different than that of the Young's modulus: for a square cross section beam, the size-dependent term in the bending modulus is $(8t/w)\Delta$, twice as big as the term $(4t/w)\Delta$ in the Young's modulus.

So, it is natural to expect some size dependence, and a number of studies have been undertaken to investigate the size dependence of the Young's modulus and other nanowire mechanical properties, as described below. However, it was not clear that the techniques that were used captured all of the relevant physics.

In this article, we provide an overview of results from an on-going first-principles study of the size dependence of the nanowire mechanical properties, especially the

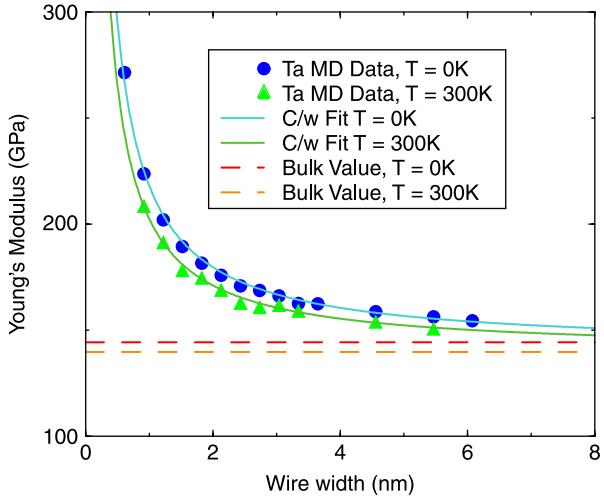

Figure 2. The Young's modulus of tantalum nanowires calculated from molecular dynamics at absolute zero and room temperature using the Finnis–Sinclair potential [16]. The wire orientation is ⟨001⟩ with {100} surfaces. Both of the curves show a size effect in which the Young's modulus increases (stiffens) as the size is reduced, with thermal softening at finite temperature.

Young's modulus. The term "first principles" in this context means that the material properties were determined from a solution of the quantum mechanics of the electrons involved in the interatomic bonds as solved by an *ab initio* approach, density functional theory (DFT). We have recently conducted what is, to the best of our knowledge, the first systematic study based on first-principles calculations of the Young's modulus of any type of nanowire [6,7]. The study, thus far, has focused on hydrogen-passivated Si ⟨001⟩ nanowires, finding that the nanowires are less stiff as their size decreases, and that the form of the size dependence is well described by existing theories. We compare to earlier calculations of the size-dependent mechanical properties predicted by atomistic simulations of nanowires using classical empirical potentials, as shown in Figure 1.

2. The mechanics of nanowires

Nanowires are being studied as mechanical components for a range of potential devices. Clamped at one or both ends, they can act as mechanical resonators for applications ranging from high frequency oscillators and filters [8] to q-bits in quantum computers [9,10]. As the device size is reduced, the frequency of the fundamental mode increases. Further miniaturization is then a way to increase the operating frequency of the oscillator. This increase in frequency can be quite desirable, provided other properties such as the quality factor of the resonator do not degrade too much. For example, the frequency of a mechanical q-bit determines the energy of its quantum state, and higher frequencies are less susceptible to decoherence from thermal fluctuations.

The basic theory governing the oscillations of a mechanical resonator is based on continuum elasticity. The theory is certainly valid for sufficiently large resonators where the materials are continuous media to a very good approximation. In limit, that the oscillating beam becomes a chain of atoms, the nature of the bonding is quite different than the bulk, and while the behavior may still be elastic, the elastic properties are expected to be significantly altered. In between, there is a range of beam sizes in which the beams are three dimensional, but the properties of the atoms on the surface may be quite different than the bulk, as described above. As the beam is miniaturized, the surfaces have an increasingly strong influence on the behavior of the beam.

The size dependence of nanowire mechanical properties has been attributed largely to these surface effects [2,4,11,12], caused specifically by surface stress and surface elastic constants. The properties of surfaces are different from those of the bulk due to the structural changes coming from the relatively unconstrained structure at the surface and modifications of the bonding environment seen in changes in the bond order. The preferred interatomic spacing at the surface may be different than that of the bulk, and the strain to form a coherent interface results in the surface stress. Similarly, the changes in the atomic interactions at the surface can result in local changes in the elastic properties expressed surface elastic constants.

3. Predictions of empirical atomistics

We have performed classical molecular dynamics simulations in order to study the elastic behavior of silicon nanowires [3,13]. These calculations are based on empirical many-body interatomic potentials, specifically the Stillinger–Weber (SW) potential [14,15] for silicon and the Finnis–Sinclair potential [16,17] for tantalum. Much of this work was done some time ago, and there have been similar results published by other groups, including one study using an empirical tight-binding method [18] that, albeit not *ab initio*, is more powerful than the classical potentials. Our purpose in reporting the empirical atomistic results here is to motivate and compare to the first-principles calculations described below.

These simulations were conducted on a system of atoms in a monatomic single crystal, apart from the surfaces, aligned such that the longitudinal axis of the simulated nanowire is the [001] crystal axis. This orientation is suitable for etched systems like nano-

electro-mechanical systems (NEMS). By contrast, nanowires that are grown often form with other orientations [19]. The nanowire spans two periodic boundaries of the simulation box, surrounded by vacuum in the transverse directions. The system was brought to mechanical and thermal equilibrium. The simulation box was expanded to stretch the nanowire, allowing the wire to relax either adiabatically at finite temperature or by steepest descent at zero temperature. The resulting stress–strain curve was fit to a fifth-order polynomial in order to calculate the Young's modulus. A typical result for the size dependence of a metal nanowire is depicted in the Young's modulus of tantalum nanowires shown in Figure 2 [13] calculated using the Finnis–Sinclair potential [16,17]. The modulus increases as the size is reduced, both at zero and room temperature. The principal temperature dependence is the thermal softening of the bulk value of the Young's modulus although there is a temperature dependence to the coefficient of the size-dependent term as well.

The size dependence of bare Si ⟨001⟩ nanowires is shown in Figure 3, based on atomistic calculations with the SW interatomic potential for silicon [14]. The zero temperature case is plotted; the effect of finite temperature is analogous to that of tantalum. A size effect is seen in both cases. As in the tantalum example, the data points are fit well by the solid curves of the form $E_0 + C/w$, where E_0 is the bulk value of the Young's modulus and w is the width of the nanowire. For the current purposes, C is a fitting constant. In principle, it is related to the surface elastic constants.

One of the more striking aspects of Figure 3 is that the sign of the surface effect is different than that for the metal in Figure 2. The SW beams soften and the Ta beams stiffen as the size is reduced. It is not surprising that the magnitude of the effect would be different in the two cases. Both potentials include many-body forces, but the Finnis–Sinclair potential includes an environmental dependence that is absent from the SW potential. Neither potential is fit to nanowire data, although the surface structures and energies calculated with the two potentials are generally reasonable and their accuracy is comparable [15]. It is an interesting question then whether the SW potential is realistic and accurate enough for meaningful calculations. Lacking suitable experimental data, we turn to first-principles calculations to make this assessment.

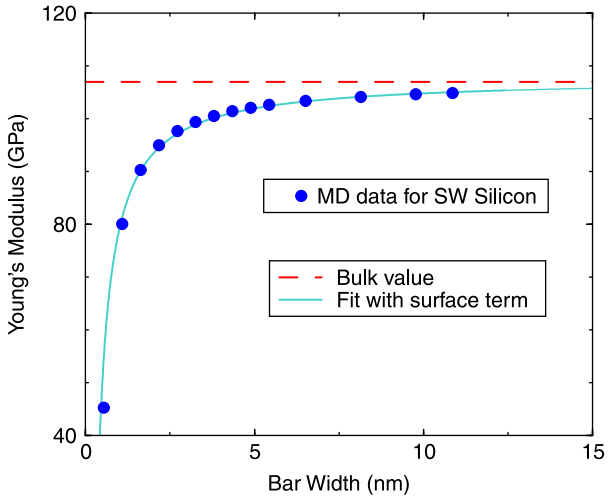

Figure 3. The Young's modulus of Si nanowires calculated from molecular dynamics at zero temperature using the SW potential. The wire orientation is ⟨001⟩ with dimer reconstructed {100} surfaces. The size effect has a different sign from that of tantalum shown in Figure 2.

4. First-principles calculations

We have calculated the Young's modulus and other mechanical properties of silicon nanowires using first-principles DFT at absolute zero temperature [6,7]. Specifically, we have employed the Vienna *ab initio* simulation package (VASP) [20,21] using the projector augmented-wave method [22,23] within the generalized gradient approximation [24]. The energy cutoff for the plane-wave expansion is 29.34 Ry and higher, and six points in the one-dimensional irreducible Brillouin zone are used for k-point sampling. Each supercell is periodic, is one Si cubic unit cell long along the hydrogen-passivated nanowire and has more than 10 Å vacuum space in the transverse directions. Computational resources have limited the size of the nanowires we can study (Appendix A). The largest nanowire, 3.92 nm in diameter, consisted of 405 Si atoms and 100 H atoms.

The nanowire simulations were constructed in a periodic box, aligned much as in the empirical atomistic calculations described above. The Si atoms were placed at the sites of a perfect Si diamond-cubic crystal and H atoms were placed above the surfaces, two per Si atom on the {100} surfaces and one per Si atom on the {110} surfaces. The dihydride Si {100} surface is known to be the ground state at low temperatures [25]. The shape of the nanowires was taken to be the Wulff shape corresponding to the surface energies for bare, reconstructed Si {100} and {110} surfaces. The bare energies were used in order to create structures suitable for comparison with bare wires, a topic of future research.

For each strain, the box dimensions were adjusted and the atoms in the nanowire were relaxed using conjugate gradient to a residual force of less than 2–10 meV/Å, where a more converged result was demanded for the smaller wires due to the larger deformations at the surface. The details of the calculations are given in Ref. [7]. The relaxed total energies were used to calculate the physical

observables: the residual stress, the equilibrium length and the Young's modulus.

4.1 Residual stress and equilibrium length

The axial stress of the nanowire constrained to be at the length corresponding to the unstrained bulk crystal (L_0) is an estimate of the residual stress that would be present in a nanowire etched from a substrate with the ends still attached to that substrate. The axial stress is determined from the derivative of the fit to the total energy as a function of strain [7]

$$\sigma_{zz}(L_0) = V^{-1}\partial U/\partial \varepsilon_{zz}|_0, \tag{7}$$

where U is the DFT total energy. It turns out that a parabolic fit describes the total energy very well for the small strains of up to a few percent that we used, so the residual stress is also equal in this approximation to the Young's modulus times the equilibrium strain. In any case, we have examined the size dependence of the residual stress and found that it is described well by the form (Refs. [6,7])

$$\sigma_{zz}(L_0) = \sigma_{zz}(\text{core}) + \frac{1}{A}\sum_i \tau_{zz}^{(i)} w_i, \tag{8}$$

where A is the cross-sectional area, w_i is the width, and $\tau_{zz}^{(i)}$ is the longitudinal surface stress, of facet i. The size dependence is thus proportional to the surface area to volume ratio. The equilibrium elongation of the larger wires also shows this scaling (Ref. [7] for details).

The surface stresses $\tau_{zz}^{(i)}$ that appear in Equation (8) were calculated from DFT total energy calculations for slabs with {100} and {110} [7]. In particular, the surface energy was calculated by subtracting the bulk contribution from the total energy of the slab in both undeformed and strained configurations. The surface stress was computed from the derivative of the surface energy with respect to the surface strain

$$\tau_{ij}^{(i)} = \frac{\partial \gamma^{(i)}}{\partial \varepsilon_{ij}}, \tag{9}$$

where $\gamma^{(i)}$ is the surface energy per unit area of the ith surface [26,27]. The expression does not include the undifferentiated surface energy, as appearing in the Shuttleworth formula for surface stress [28], and the two sides of Equation (8) agree only if such a term is omitted. Recently, this form for the surface stress has also been found to work for other solid state systems [29].

4.2 Young's modulus

The Young's modulus is calculated from the second derivative of the relaxed total energy as a function of strain. The results are shown in Figure 4. The square symbols denote the first-principles results. The Young's modulus softens as the size of the nanowire is reduced, as was seen for the SW atomistic calculations above. The + signs denote the results of a continuum model parameterized with DFT data derived entirely from bulk and surface slab calculations, rather than the more computationally expensive explicit nanowire geometry. The dashed curve denotes the results of a fit to published molecular statics calculations based on the SW potential [4] for 1 × 1 Si {100} wires. The solid curve represents a fit to $E_0 + C/w$ where E_0 is the Young's modulus of the bulk crystal and w is the width of the nanowire. Even though the 1 × 1 {100} surface is not the ground state and the calculation is therefore contrived, it may be a better analog of the H passivated wire than the more realistic 2 × 1 bare wires of Figures 1 and 3.

The comparison of the Young's modulus of a hydrogen-passivated Si nanowire calculated with DFT to the Young's modulus of a bare Si nanowire calculated with empirical atomistics is not a direct comparison; nevertheless, it is interesting that the SW potential is reasonably close to the first-principles result. It does not contain any physics characteristic of the surface, such as a change in the bond character. Of course, the effect of the H passivation is to mitigate some of the environmental dependence that more sophisticated potentials are designed to capture. We need the results of DFT calculations for bare wires to make a direct comparison.

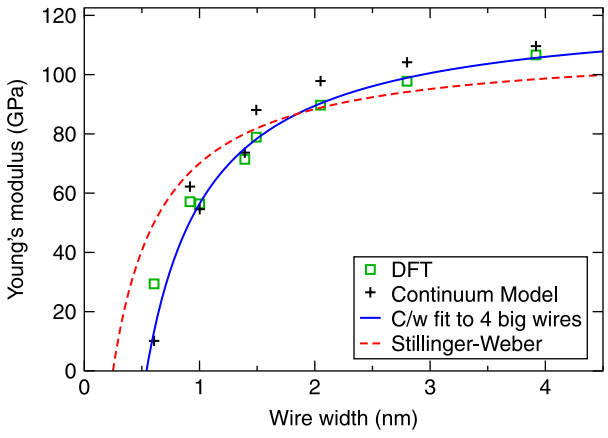

Figure 4. The Young's modulus of hydrogen-passivated Si ⟨001⟩ nanowires calculated from first principles in DFT [7]. The square symbols denote the DFT results. For comparison, three other values are plotted, as described in the text.

5. Conclusion and outlook

We have studied the mechanics of Si nanowires using first-principles techniques. The results on the size dependence of the Young's modulus are consistent with the dominant contribution coming from surface effects, as verified from comparison to a continuum model parameterized with data from first-principles calculations of bulk and slab systems. Recently, there have been increasing experimental efforts to measure the size dependence of the nanowire Young's modulus for several materials [30–35]. The vast majority of these nanowires are much larger than the ones we have studied. Computational limitations prevent us from calculating the modulus of the larger wires, but scaling up from our results would suggest that the effect would be negligible for hydrogen-passivated Si ⟨001⟩ larger than 10 nm.

There are many questions that remain open regarding the nanowire mechanics. There are some hints that effects from sources other than surfaces are important in the smallest wires we have studied. The hydrogen-passivated surfaces are among the most benign possible, so it is natural to ask whether the threshold for these anomalies occurs at a larger size for other types of surfaces. The exact nature of these effects is unknown. Even for the more conventional surface effects, we still do not have an understanding of the physics that is sufficiently powerful to allow us to derive an effective interatomic potential that reproduces the first-principles behavior. Some efforts have begun along these lines [36], but clearly much more is needed in terms of theory, development and validation.

Acknowledgements

We are grateful to Livermore Computing for extensive supercomputer resources on MCR, Thunder, Atlas and Zeus. This work was performed under the auspices of the US Department of Energy by Lawrence Livermore National Laboratory under Contract DE-AC52-07NA27344. R.E.R. gratefully acknowledges the support of the National Science Foundation through NIRT Grant Award No. CMS-0404031.

Note

1. When the Poisson ratios differ, $\nu_{\text{core}} \neq \nu_{\text{surf}}$, the formula is $\Delta = [E_{\text{surf}} - E_{\text{core}} + E_{\text{surf}}\nu_{\text{core}}(\nu_{\text{core}} - \nu_{\text{surf}})/(1 - \nu_{\text{surf}}^2)]/E_{\text{core}}$.

References

[1] D.K. Allen, *Metallurgy Theory and Practice*, American Technical Publishers, Homewood, Ill, 1969.
[2] J.Q. Broughton, C.A. Meli, P. Vashishta, and R.K. Kalia, *Direct atomistic simulation of quartz crystal oscillators: bulk properties and nanoscale devices*, Phys. Rev. B 56 (1997), p. 611.
[3] R.E. Rudd and J.Q. Broughton, *Atomistic simulation of MEMS resonators through the coupling of length scales*, J. Mod. Sim. Microsys. 1 (1999), p. 29.
[4] R.E. Miller and V.B. Shenoy, *Size-dependent elastic properties of nanosized structural elements*, Nano Tech. 11 (2000), p. 139.
[5] S.P. Timoshenko and J.N. Goodier, *Theory of Elasticity*, 3rd ed., McGraw-Hill, New York, 1970.
[6] B. Lee and R.E. Rudd, *First principles study of the Young's modulus of Si ⟨001⟩ nanowires*, Phys. Rev. B (2007), 041305(R).
[7] B. Lee and R.E. Rudd, *First-principles calculation of mechanical properties of Si ⟨001⟩ nanowires and comparison to nanomechanical theory*, Phys. Rev. B 75 (2007), 195328.
[8] A.N. Cleland and M.L. Roukes, *Fabrication of high frequency nanometer scale mechanical resonators from bulk Si crystals*, Appl. Phys. Lett. 69 (1996), 2653.
[9] A.N. Cleland and M.R. Geller, *Superconducting qubit storage and entanglement with nanomechanical resonators*, Phys. Rev. Lett. 93 (2004), 070501.
[10] M. Blencowe, *Quantum electromechanical systems*, Phys. Rep. 395 (2004), p. 159.
[11] J.W. Cahn, *Surface stress and the chemical equilibrium of small crystals-I. The case of the isotropic surface*, Acta Metall. 28 (1980), p. 1333.
[12] H. Liang, M. Upmanyu, and H. Huang, *Size-dependent elasticity of nanowires: nonlinear effects*, Phys. Rev. B (2005), 241403(R).
[13] R.E. Rudd, *Coarse-grained molecular dynamics for computer modeling of nanomechanical systems*, Int. J. Multiscale Comp. Eng. 2 (2004), p. 203.
[14] F.H. Stillinger and T.A. Weber, *Computer simulation of local order in condensed phases of silicon*, Phys. Rev. B 31 (1985), p. 5262.
[15] H. Balamane, T. Halicioglu, and W.A. Tiller, *Comparative study of silicon empirical interatomic potentials*, Phys. Rev. B 46 (1992), p. 2250.
[16] M. Finnis and J. Sinclair, *A simple empirical* N*-body potential for transition metals*, Phil. Mag. A 50 (1984), p. 45.
[17] G.J. Ackland et al., *An improved* N*-body semi-empirical model for bcc transition metals*, Phil. Mag. A 56 (1987), p. 15.
[18] D.E. Segall, S. Ismail-Beigi, and T.A. Arias, *Elasticity of nanometer-sized objects*, Phys. Rev. B 65 (2002), 214109.
[19] C.M. Lieber, *Nanoscale science and technology: building a big future from small things*, MRS Bull. 28 (2003), p. 486.
[20] G. Kresse and J. Furthmüller, *Efficient iterative schemes for ab initio total-energy calculations using a plane-wave basis set*, Phys. Rev. B 54 (1996), p. 11169.
[21] G. Kresse and J. Furthmüller, *Efficiency of* ab-initio *total energy calculations for metals and semiconductors using a plane-wave basis set*, Comp. Mat. Sci. 6 (1996), p. 15.
[22] P.E. Blöchl, *Projector augmented-wave method*, Phys. Rev. B 50 (1994), p. 17953.
[23] G. Kresse and D. Joubert, *From ultrasoft pseudopotentials to the projector augmented-wave method*, Phys. Rev. B 59 (1999), p. 1758.
[24] J.P. Perdew, K. Burke, and M. Ernzerhof, *Generalized gradient approximation made simple*, Phys. Rev. Lett. 77 (1996), p. 3865.
[25] S. Ciraci and I.P. Batra, *Theory of transition from the dihydride to the monohydride phase on the Si(001) surface*, Surf. Sci. 178 (1986), p. 80.
[26] M.E. Gurtin and A.I. Murdoch, *A continuum theory of elastic material surfaces*, Arch. Rat. Mech. Anal. 57 (1975), p. 291.
[27] R.V. Kukta, D. Kouris, and K. Sieradzki, *Adatoms and their relation to surface stress*, J. Mech. Phys. Solids 51 (2003), p. 1243.
[28] R. Shuttleworth, *The surface tension of solids*, Proc. Phys. Soc. A 63 (1950), p. 444.
[29] W.G. Wolfer, *Private communication* (2007)
[30] E.W. Wong, P.E. Sheehan, and C.M. Lieber, *Nanobeam mechanics: elasticity, strength, and toughness of nanorods and nanotubes*, Science 277 (1997), p. 1971.
[31] S. Cuenot, C. Fretigny, S. Demoustier-Champagne, and B. Nysten, *Surface tension effect on the mechanical properties of nanomaterials measured by atomic force microscopy*, Phys. Rev. B 69 (2004), 165410.

[32] C.Q. Chen, Y. Shi, Y.S. Zhang, J. Zhu, and Y.J. Yan, *Size dependence of Young's modulus in ZnO nanowires*, Phys. Rev. Lett. 96 (2006), 075505.
[33] X.Q. Chen, S.L. Zhang, G.J. Wagner, W.Q. Ding, and R.S. Ruoff, *Mechanical resonance of quartz microfibers and boundary condition effects*, J. Appl. Phys. 95 (2004), p. 4823.
[34] T. Kizuka, Y. Takatani, K. Asaka, and R. Yoshizaki, *Measurements of the atomistic mechanics of single crystalline silicon wires of nanometer width*, Phys. Rev. B 72 (2005), 035333.
[35] A. San Paulo, J. Bokor, R.T. Howe, R. He, P. Yang, D. Gao, C. Carraro, and R. Maboudian, *Mechanical elasticity of single and double clamped silicon nanobeams fabricated by the vapor–liquid–solid method*, Appl. Phys. Lett. 87 (2005), 053111.
[36] B. Lee and K. Cho, *Extended embedded-atom method for platinum nanoparticles*, Surf. Sci. 600 (2006), p. 1982.
[37] E.R. Davidson, *Matrix eigenvector methods in quantum mechanics*, in *Methods in Computational Molecular Physics*, G.H.F. Diercksen and S. Wilson, eds., Reidel, Dordrecht, The Netherlands, 1983, pp. 95–113.
[38] B. Liu, *Numerical algorithms in chemistry: algebraic methods*, in *Report on Workshop*, C. Moler and I. Shavitt, eds., Lawrence Berkley Lab, Berkeley, CA, LBL-8158 1978, p. 49.

Appendix A Supercomputer considerations

The calculation of the mechanical properties of the nanowires studied here with DFT requires supercomputer resources in order to complete the calculation in a tolerable amount of time. The DFT calculations scale roughly as N^3 where N is the number of electrons. In practice, the scaling can be substantially worse than this due to various computational overheads. For example, the largest nanowire we have studied, 3.92 nm in diameter, consisted of 405 Si atoms and 100 H atoms. This one wire required over 100,000 CPU hours of computation on up to 512 CPUs of the MCR supercomputer (described below). The 2.05-nm nanowire, although only about a factor of 2 smaller in radius or a factor of 3.5 smaller in the number of electrons, took about 1% of this time, less than half of the N^3-scaled time. With the computational cost for large wires rising rapidly with the size, we were limited in the wire sizes that could be studied. Also some care was needed in how the calculation of the larger wires was performed.

Several questions at the Nanotech'07 conference were focused on how these supercomputer calculations were conducted and the performance that was attained. We report some of those properties in this appendix.

The calculations have been performed on several supercomputers. Most of the big calculations were done on the MCR supercomputer at Lawrence Livermore National Laboratory (LLNL). It has since been retired, but it had 2304 Intel Xeon (32 bit, 2.4 GHz) processors organized in 1152 dual-processor nodes reaching a peak performance of 11.2 Tflop/s. Communications were done through a high performance interconnect from Quadrics.

More recently, the calculations have been performed on the Thunder and Zeus supercomputers at LLNL. Thunder is a Linux machine with 4096 Intel Itanium2 (64 bit, 1.4 GHz) processors distributed with four processors on each of 1024 nodes. Its peak capacity is 22.9 Tflop/s. Its communications are done through a Quadrics switch. Zeus is also a Linux machine with 2304 cores (CPUs) on AMD Opteron (64 bit, 2.4 GHz) chips organized with eight cores on each of 288 nodes and a peak capacity of 11.1 Tflop/s. Its communications are done through an InfiniBand switch.

The strong scaling performance on the Zeus supercomputer is shown in Figure 5. Here, performance scaling is simply defined as the ratio of CPU time taken on single node to the time taken on N nodes for the given calculation. Perfect scaling would be a value of N for N nodes; values less than perfect are generally due to the cost of communications and redundant calculation.

The self-consistent loop in the VASP code [20] solves the Schrödinger Equation defined as

$$\hat{H}|\psi_n\rangle = \varepsilon_n|\psi_n\rangle, \tag{A1}$$

where $|\psi_n\rangle$ is an eigenstate (nth band) of the Kohn-Sham Hamiltonian, and ε_n is the corresponding eigenenergy. Using a plane-wave basis set, an eigenstate can be expanded as

$$|\psi_n\rangle = \sum_q C_{nq}|q\rangle, \tag{A2}$$

where C_{nq} is the coefficient of a plane-wave component $|q\rangle$. The simplest way to solve this eigenvalue problem is to diagonalize the entire matrix directly, which effectively distributes the calculation of C_{nq} as evenly as possible to nodes. The direct diagonalization ("Direct" in Figure 5) reveals that the increasing communication overhead, as the number of nodes is increased, significantly brings down the performance scaling: the efficiency of using eight nodes (64 cores) is about 50%, i.e. essentially no speed-up results from adding more nodes beyond four nodes.

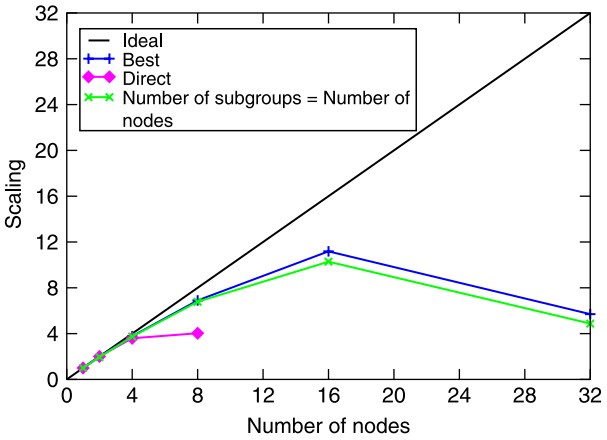

Figure 5. Scaling of the computational performance as a function of the number of nodes on the Zeus supercomputer. Each node contains eight cores (CPUs). The number of subgroups involves how the calculation is organized (see text). The 2.05-nm wire (109 Si atoms and 52 H atoms) has been used, and the result may not be directly transferable to a system with substantially different size. Similar performance trends were found on other supercomputers, although the hardware architecture does have an effect on the optimal parameters for the calculation.

Another strategy for parallelization is to divide the matrix into subspaces, optimize subspaces first, and then diagonalize the assembled matrix [37,38]. Since this approach allows us to work on smaller spaces, the communication overhead mentioned above is significantly reduced. Nevertheless, it necessarily increases the number of calculation steps and memory requirements, and also introduces additional communication necessary to keep the eigenstates in subspaces orthogonalized.

Therefore, the optimal performance for the given number of nodes is determined from the competition between two different communication overheads. The optimum is also strongly tied to the supercomputer architecture, but it turns out that the performance is generally good when the number of subgroups is comparable to the number of nodes on Zeus.

The best performance also depends on the system size on top of all the factors mentioned above, and it is achieved on 16 nodes and eight subgroups, with 70% efficiency compared to the ideal number, for the 2.05-nm wire.